Effect of Vacancy on Physical Properties of *Cmcm* Si_{24}

M. Jia[a], Q. Fan[a,b,*], B. Hao[a],
Y. Zhao[c], Y. Song[d] and S. Yun[e]

[a] *College of Science, Xi'an University of Architecture and Technology, Xi'an, 710055, China*
[b] *College of Information and Control Engineering, Xi'an University of Architecture and Technology, Xi'an 710055, China*
[c] *School of Mechanical and Electrical Engineering, Xi'an University of Architecture and Technology, Xi'an, 710055, PR China*
[d] *School of Microelectronics, Xidian University, Xi'an 710071, China*
[e] *Functional Materials Laboratory (FML), School of Materials Science and Engineering, Xi'an University of Architecture and Technology, Xi'an, 710055, PR China*

Received: 01.11.2023 & Accepted: 12.02.2024

Doi: 10.12693/APhysPolA.145.235 *e-mail: fanqy@xauat.edu.cn

Researchers recently synthesized a new orthorhombic allotrope of silicon, namely *Cmcm* Si_{24}. This work studied the effect of one vacancy for *Cmcm* Si_{24} on structural, electronic, and mechanical anisotropy properties by the first principle calculation. The lattice parameters of *Cmcm* Si_{24}:V are the same as *Cmcm* Si_{24}, but the density of *Cmcm* Si_{24}:V is larger than that of *Cmcm* Si_{24}. Moreover, the values of elastic moduli for *Cmcm* Si_{24}:V are smaller than for *Cmcm* Si_{24}. The *Cmcm* Si_{24}:V has mechanical stability and anisotropy and has lower formation energy than diamond-Si. The analysis of the band structures shows that *Cmcm* Si_{24} is an indirect band gap material, and the value of the band gap is 1.08 eV. In particular, electronic band structures of *Cmcm* Si_{24}:V exhibit metallic characteristics. Furthermore, the electron localization function indicated strong covalent silicon–silicon bonds in *Cmcm* Si_{24} and *Cmcm* Si_{24}:V. In addition, the effective mass of electrons and holes of *Cmcm* Si_{24} is smaller than that of diamond-Si along the *a* direction, and larger than that along the *b* and *c* directions. Finally, the X-ray diffraction patterns for *Cmcm* Si_{24} and *Cmcm* Si_{24}:V are very close after 13.84°.

topics: silicon allotropes, crystal-structure prediction, first-principles method, X-ray diffraction (XRD)

1. Introduction

Since the continuous progress of the new energy industry, solar energy, with great potential for development, has been widely discussed [1]. Due to the rapid development of computational materials science, many related materials such as carbon, silicon, germanium, and some metal alloys have been explored [2–6]. For decades, silicon-based photovoltaic devices dominated the solar cell industry due to their great stability, environmentally friendliness, superior efficiency of photoelectric conversion, and technical advantages. *Fd*-3*m*-Si (diamond phase) dominates the solar cell market. Nevertheless, *Fd*-3*m*-Si has an indirect band gap, and the energy difference between the direct and indirect band gap is up to 2.3 eV, which makes diamond silicon have a lower absorption efficiency. This has limited the application of silicon in the optoelectronics industry to a certain extent [7–9] because the direct band gap materials are able to carry out quick response and high efficiency for optoelectronic devices.

Although more and more researchers are interested in the other allotropes and alloys [10–17], a number of researchers keep searching for silicon allotropes that have direct band gaps or excellent material properties. Through continuous efforts, the researchers predicted a lot of silicon allotropes [18–34]. However, the majority of them still have indirect band gaps. The silicon allotrope, h-Si_6, which has a 0.61 eV direct band gap, was proposed by Guo et al. [26]. The solar absorption capacity, as well as electron transport characteristics, of h-Si_6 are satisfactory. In addition, Cai et al. [33] predicted a direct band gap allotrope (*tP*36-Si) with 0.58 eV through first-principles calculation, and its optical performance is superior to diamond-Si. Furthermore, Fan et al. [34] discovered *cm*-32 silicon and $P2_1/m$ silicon with a direct band gap. These two silicon allotropes have good photovoltaic efficiency and are suitable for thin-film solar cells. Moreover, He et al. [19] used first-principles calculations to study the stability and physical properties of five sp^3 hybrid silicon allotropes. The results

show that all S-Si, Z-CACB-Si, H-Si, and Z-ACA-Si have quasi-direct band gaps, while M585-Si has a direct band gap of 1.51 eV.

Recently, Kim et al. [35] have synthesized a new orthorhombic silicon allotrope from the removing sodium atom Na_4Si_{24} precursor. They found that the new silicon phase has $Cmcm$ symmetry and Si_{24} is a semiconductor material with a 1.3 eV indirect band gap value. Therefore, we studied the effect of vacancy for Si_{24} in the $Cmcm$ phase on this basis and used $Cmcm$ Si_{24}:V to represent this structure in the following text. The crystal structure and mechanical, and electronic properties of $Cmcm$ Si_{24}:V were investigated in this work.

2. Computational method

The calculations in this study are implemented by the Cambridge Sequential Total Energy Package (CASTEP) code [36] based on density functional theory (DFT) [37–38]. The generalized gradient approximation (GGA) parameterized by Perdew–Burke–Ernzerhof (PBE) [39] performed exchange and correlation functional. The Broyden–Fletcher–Goldfarb–Shanno (BFGS) [40] minimization optimized the geometry. The interaction between electrons and ions is described by ultrasoft quasi-potential [41] in the calculation. Meanwhile, the wave energy cutoff value of $Cmcm$ Si_{24} and $Cmcm$ Si_{24}:V is 340 eV. In Brillouin zone sampling, the spacing of the k-point Monkhorst–Pack [42] grid is approximately $2\pi \times 0.025$ Å^{-1}. All these ensure good convergence of energy and computational structure in this work. In addition, the elastic moduli, including the bulk, shear, and Young's modulus, are estimated by the Voigt–Reuss–Hill approximation method [43]. Furthermore, the electronic band structures based on Heyd–Scuseria–Ernzerhof (HSE06) hybrid functional [44] are obtained by using the PWmat [45, 46], and the electron localization function (ELF) is studied by using the MedeA VASP [47, 48].

3. Results and discussion

The number of possible crystal structures for $Cmcm$ Si_{24}:V is 24, and we then select the most stable possible structure to investigate its physical properties. The crystal structure for $Cmcm$ Si_{24} and $Cmcm$ Si_{24}:V are shown in Fig. 1. For $Cmcm$ Si_{24}, there are three inequivalent silicon atoms that occupy the crystallographic $8f$ sites, namely $8f$ (0.00000, 0.24341, 0.55461), $8f$ (0.00000, 0.57049, 0.34279), and $8f$ (0.00000, 028753, 0.59015). The red, orange, and pink spheres represent Si1, Si2, and Si3 atoms, respectively. In Fig. 1b, the position of atoms missing for one vacancy is seen clearly. The missing atom position of one vacancy is Si1 (1.00000, 0.24340, 0.55461). Furthermore, the position of the $Cmcm$ Si_{24}:V is consistent with previous

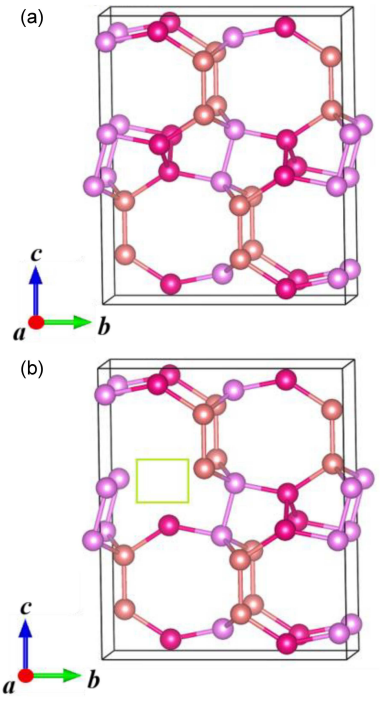

Fig. 1. The crystal structures of $Cmcm$ Si_{24} (a) and $Cmcm$ Si_{24}:V (b).

TABLE I

The density [g/cm^3] and lattice parameters [Å] for $Cmcm$ Si_{24} and $Cmcm$ Si_{24}:V.

Material	Method	ρ	a	b	c	Ref.
Si_{24}	PBE	1.714	3.858	10.762	12.789	this work
			3.848	10.744	12.734	[35]
			3.822	10.701	12.626	exper. [35]
Si_{24}:V	PBE	2.020	3.848	10.477	12.814	this work

report [49]. The lattice parameters and density for $Cmcm$ Si_{24} and $Cmcm$ Si_{24}:V are listed in Table I (see also [35]), along with the calculated theoretical values and experimental values for $Cmcm$ Si_{24}. The lattice parameters of $Cmcm$ Si_{24} are in compliance with the experimental values [35] in Table I, demonstrating the credibility of the theoretical results obtained in this work. As seen in Table I, the lattice parameters a and b of $Cmcm$ Si_{24}:V are smaller than those of $Cmcm$ Si_{24}, while c of $Cmcm$ Si_{24}:V is larger. The results show that the presence of vacancy changes the lattice parameters and density of $Cmcm$ Si_{24}, and the density of $Cmcm$ Si_{24}:V is larger than that of $Cmcm$ Si_{24}.

The elastic constants, bulk modulus B, shear modulus G, and Young's modulus E for $Cmcm$ Si_{24} and $Cmcm$ Si_{24}:V are also researched in the paper, and the results are listed in Table II. There are nine independent elastic constants for orthorhombic crystal, namely C_{11}, C_{12}, C_{13}, C_{22}, C_{23}, C_{33}, C_{44}, C_{55}, and C_{66}. Therefore, the stable structure for an orthorhombic system should meet the following necessary and sufficient Born's mechanical

TABLE II

The elastic constants [GPa] and elastic modulus [GPa] for *Cmcm* Si_{24} and *Cmcm* Si_{24}:V.

	C_{11}	C_{12}	C_{13}	C_{22}	C_{23}	C_{33}	C_{44}	C_{55}	C_{66}	B	G	E
Si_{24}	162	32	33	189	39	140	46	48	53	77	54	132
Si_{24}:V	136	31	32	146	35	110	33	45	30	65	40	99

stability criteria: $C_{11} > 0$, $C_{11}C_{22} > C_{12}^2$, $C_{11}C_{22}C_{33} + 2C_{12}C_{13}C_{23} - C_{11}C_{23}^2 - C_{22}C_{13}^2C_{33}C_{12}^2 > 0$, $C_{44} > 0$, $C_{55} > 0$, $C_{66} > 0$ [50]. Obviously, the independent elastic constants for *Cmcm* Si_{24} and *Cmcm* Si_{24}:V in Table II satisfy the orthorhombic symmetry generalized Born's mechanical stability criteria. This demonstrates the mechanical stability of *Cmcm* Si_{24} and *Cmcm* Si_{24}:V.

To determine whether the native defects are easily formed in *Cmcm* Si_{24}, the calculation of formation energy and defect formation energy is imperative. The formation energy (ΔE) for *Cmcm* Si_{24} and *Cmcm* Si_{24}:V is defined as

$$\Delta E = E_{Cmcm\,\text{phase}}/m - E_{\text{diamond phase}}/n, \quad (1)$$

where $E_{Cmcm\,\text{phase}}$ is the total energy of the crystals at equilibrium lattice constant; $E_{\text{diamond phase}}$ is the energy of diamond Si; m represents the number of atoms in the conventional cell of the *Cmcm* phase, so it is equal to 24 and 23, respectively; n is equal to 8. The definition of defect formation energy is

$$\Delta E_f = E_{\text{defect}} - E_{perfect} + \sum_i n_i\mu_i, \quad (2)$$

where E_{defect} is the total energy of defective supercell; $E_{perfect}$ is the total energy of perfect intrinsic supercell; n_i represents the number of atoms (i) removed from ($n_i > 0$) or added to ($n_i < 0$) the perfect supercell, and μ_i represents the chemical potential of the corresponding atom.

Table III (see also [51]) listed the results of formation energy and defect formation energy for *Cmcm* Si_{24}, diamond-Si:V, and *Cmcm* Si_{24}:V. The formation energy ΔE of Cmcm Si_{24}, *Cmcm* Si_{24}:V, and diamond-Si:V are 0.089, 0.217, and 0.417 eV/atom, respectively. The defect formation energy ΔE_f of *Cmcm* Si_{24}:V and diamond-Si:V are 4.315 and 4.438 eV. For diamond-Si:V, the calculated ΔE_f is 4.438 eV, which is not significantly different from the 4.01 eV value proposed in previous literature [51], which proves the accuracy and effectiveness of our calculation. Actually, we all know that it is easier to form low-energy structures. As shown in Table III, the defect formation energy of diamond-Si:V is similar to that of *Cmcm* Si_{24}:V. However, the formation energy of *Cmcm* Si_{24}:V is much lower than the formation energy for diamond-Si:V; this illustrates the synthesized possibility for vacancy in the *Cmcm* Si_{24}.

The bulk modulus and shear modulus are estimated according to the obtained elastic constants, and Young's modulus is estimated from the value of bulk modulus and shear modulus by $E = 9BG/(3B + G)$ [43]. As shown in Table II, the presence of vacancy changes the elastic moduli of *Cmcm* Si_{24}, and the values of B, G, and E for *Cmcm* Si_{24}:V are all smaller than for *Cmcm* Si_{24}. The bulk modulus of *Cmcm* Si_{24} is 77 GPa, the shear modulus is 54 GPa, and the Young's modulus is 132 GPa. Moreover, the B, G, and E values of *Cmcm* Si_{24}:V are 65, 40, and 99 GPa, respectively. For the purpose of further study of the influence of vacancy on the anisotropy of elastic modulus of structure, the three-dimensional (3D) surface constructions of Young's modulus are investigated

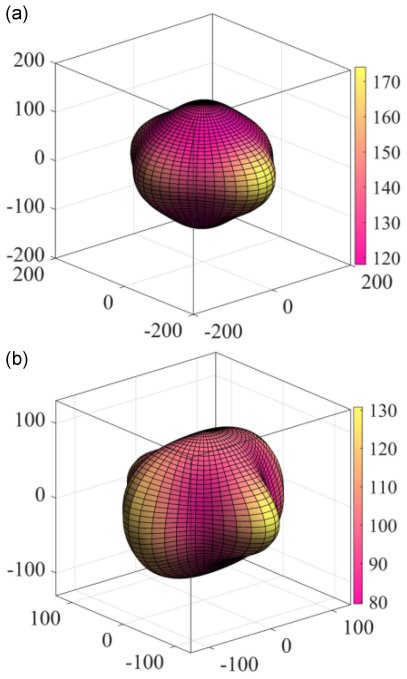

Fig. 2. The three-dimensional directional dependence of Young's modulus for *Cmcm* Si_{24} (a) and *Cmcm* Si_{24}:V (b).

TABLE III

The formation energies and defect formation energies for *Cmcm* Si_{24}, diamond-Si:V, and *Cmcm* Si_{24}:V.

	Vacancy	ΔE [eV/atom]	ΔE_f [eV]	Ref.
Si_{24}	zero	0.089		this work
	one	0.217	4.315	this work
diamond-Si	one	0.417	4.348	this work
diamond-Si	one		4.01	[51]

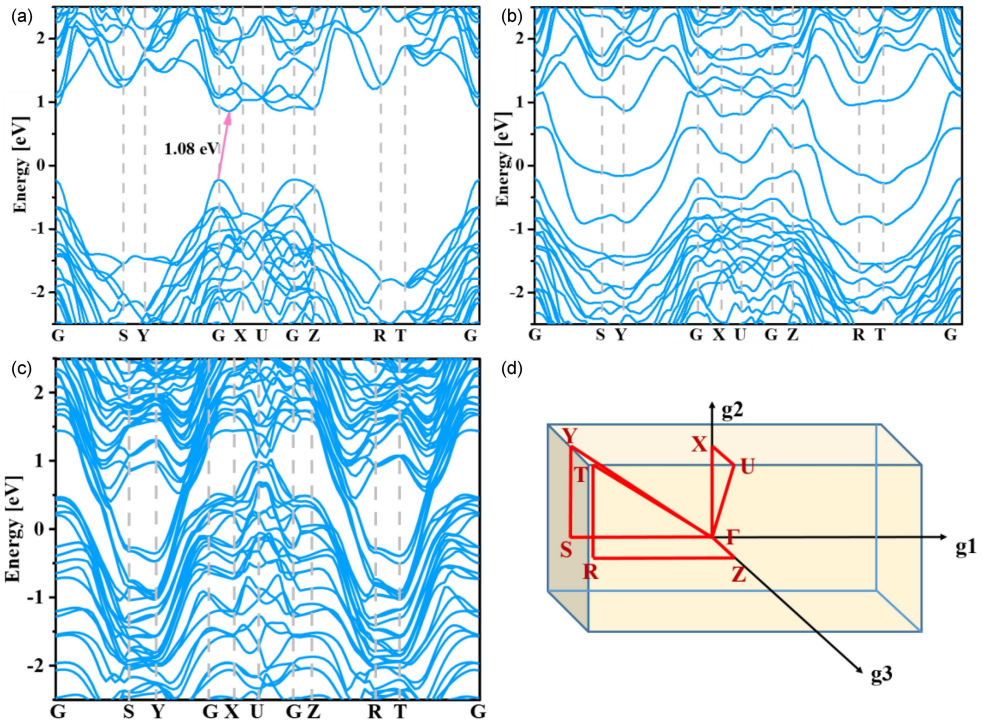

Fig. 3. The band structures of *Cmcm* Si_{24} (a), *Cmcm* Si_{24}:V in one cell (b), *Cmcm* Si_{24}:V in $1 \times 1 \times 3$ supercell (c), and the Brillouin zone for *Cmcm* Si_{24} and *Cmcm* Si_{24}:V (d).

in this work. Figure 2 shows the 3D directional dependence of Young's modulus for *Cmcm* Si_{24} and *Cmcm* Si_{24}:V. The 3D figure of an isotropic structure exhibits a spherical shape, while the anisotropy degree is represented by deviation from the spherical shape. The deformed spheres plotted in Fig. 2 show that *Cmcm* Si_{24} and *Cmcm* Si_{24}:V have mechanical anisotropy, and the anisotropy of *Cmcm* Si_{24}:V is greater than *Cmcm* Si_{24}.

Since band structures are able to depict the electronic properties of crystals, in this work, the electronic band structures are investigated by using the HSE06 function and PWmat. Figure 3 displays the band structures and Brillouin zone for *Cmcm* Si_{24} and *Cmcm* Si_{24}:V. Figure 3d shows the Brillouin zone of Si_{24}; the coordinates of high symmetry points across the Brillouin zone for *Cmcm* Si_{24} and *Cmcm* Si_{24}:V are G $(0.0, 0.0, 0.0)$ $\rightarrow$ S $(-0.5, 0.0, 0.0)$ $\rightarrow$ Y $(-0.5, 0.5, 0.0)$ $\rightarrow$ G $(0.0, 0.0, 0.0)$ $\rightarrow$ X $(0.0, 0.5, 0.0)$ $\rightarrow$ U $(0.0, 0.5, 0.5)$ $\rightarrow$ G $(0.0, 0.0, 0.0)$ $\rightarrow$ Z $(0.0, 0.0, 0.5)$ $\rightarrow$ R $(-0.5, 0.0, 0.5)$ $\rightarrow$ T $(-0.5, 0.5, 0.5)$ $\rightarrow$ G $(0.0, 0.0, 0.0)$. As can be seen in Fig. 3a, *Cmcm* Si_{24} is a semiconductor material with an indirect band gap of 1.08 eV, the conduction band minimum (CBM) of *Cmcm* Si_{24} is between the G point and the X point, while the valence band maximum (VBM) is located at the G point. Compared with *Cmcm* Si_{24}, the presence of vacancy has a great impact on electronic band structures. In particular, the *Cmcm* Si_{24}:V exhibits metallic characteristics in electronic band structures. VBM for *Cmcm* Si_{24}:V is located at the Z point, while its conduction bands along G–S–Y–G and Z–G directions exhibit metallic characteristics since the bottom dispersive band crosses into the region below Fermi level with negative energy. In order to avoid the problem of band anomalies caused by high defect concentration, we conducted band calculations on supercells that expand three times along the direction a in Fig. 1, as shown in Fig. 3c. We found that the band gap of the band structure in Fig. 3c is indeed narrower than that in Fig. 3b, but both band structures exhibit metallic properties. To further illustrate the chemical bonding in *Cmcm* Si_{24} and *Cmcm* Si_{24}:V, the electron localization function (ELF) using an isosurface value of 0.8 are exhibited in Fig. 4. The high ELF values with symmetric shapes at the bond centers indicated strong covalent silicon–silicon bonds.

Effective mass is one of the important indicators for grading the transport performance of semiconductors, and it is in a position to provide a theoretical basis for the crystal orientation design of semiconductor devices by analysis of its anisotropy. The effective masses of *Cmcm* Si_{24} are calculated by using the relation

$$\frac{1}{m^*} = \frac{1}{\hbar^2}\frac{\partial^2 E}{\partial k^2}. \tag{3}$$

The effective masses of holes and electrons for diamond-Si and *Cmcm* Si_{24} along the a, b, and c axes are given in Table IV (see also [48, 49]).

TABLE IV

Effective masses of holes and electrons (in m_0) for diamond-Si and *Cmcm* Si_{24} along the *a*, *b*, and *c* directions.

Material	Electron effective mass			Hole effective mass			Ref.
	a direction	*b* direction	*c* direction	*a* direction	*b* direction	*c* direction	
diamond-Si	0.916	0.191	0.191	0.460 (heavy) 0.171 (light)	0.460 (heavy) 0.171 (light)	0.460 (heavy) 0.171 (light)	exper. [48, 49]
	0.926	0.195	0.195	0.268 (heavy) 0.178 (light)	0.268 (heavy) 0.178 (light)	0.268 (heavy) 0.178 (light)	this work
Si_{24}	0.129	0.608	1.344	0.136	0.465	2.004	this work

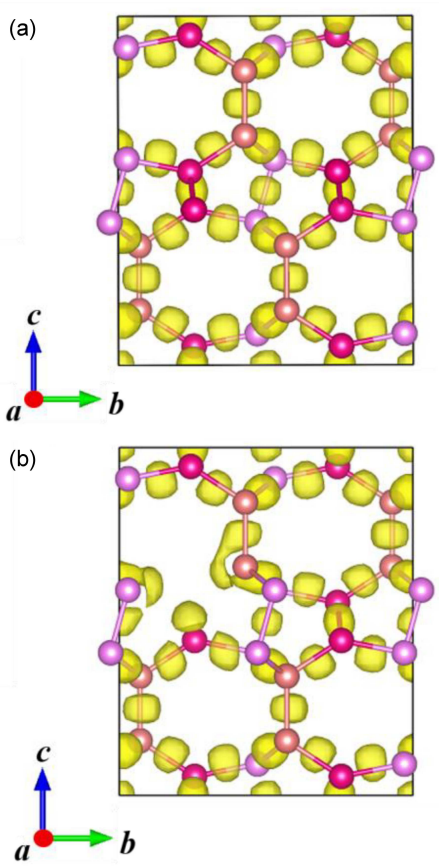

Fig. 4. ELF for *Cmcm* Si_{24} (a) and *Cmcm* Si_{24}:V (b) with an isosurface level set to 0.8.

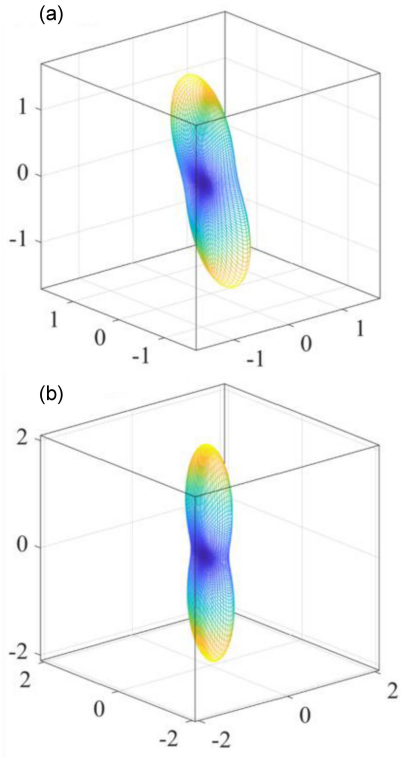

Fig. 5. Three-dimensional contour plots of the effective masses (in m_0) of electrons (a) and holes (b) of *Cmcm* Si_{24}.

The calculated effective mass of diamond-Si is consistent with the reported experimental results, proving the reliability of our research results. The effective mass of electrons and holes of *Cmcm* Si_{24} is smaller than diamond-Si along the *a* direction and larger than that along the *b* and *c* directions. In order to analyze the anisotropy and directionality of material effective mass more directly, we plotted the three-dimensional (3D) representation diagram of effective mass in Fig. 5. The 3D shapes of the electrons and holes effective mass of *Cmcm* Si_{24} are tall and slender. These results indicated the greater anisotropy of the effective mass of electrons and holes of *Cmcm* Si_{24} than that of diamond-Si.

An X-ray wavelength of 1.5406 Å and a copper source are used in this work to simulate the X-ray diffraction (XRD) patterns. The XRD patterns for *Cmcm* Si_{24} and *Cmcm* Si_{24}:V are displayed in Fig. 6. It can be seen from the diffraction peaks after 13.84° that the XRD spectra for *Cmcm* Si_{24} and *Cmcm* Si_{24}:V are very close. There are many diffraction peaks in XRD patterns of *Cmcm* Si_{24}, and several peaks of the main diffraction peaks marked in the figure are (002), (020), (021), (022), and (113). The (002), (020), (021), and (022) peaks are located at the diffraction angles of 13.84°, 16.46°, 17.87°, and 21.57°, respectively. The (113) peak is located around 32.35°, and the diffraction angles of 47.05° has the (200) peak. Compared with *Cmcm* Si_{24}, the XRD patterns before 13.84° of *Cmcm* Si_{24}:V has four diffraction peaks,

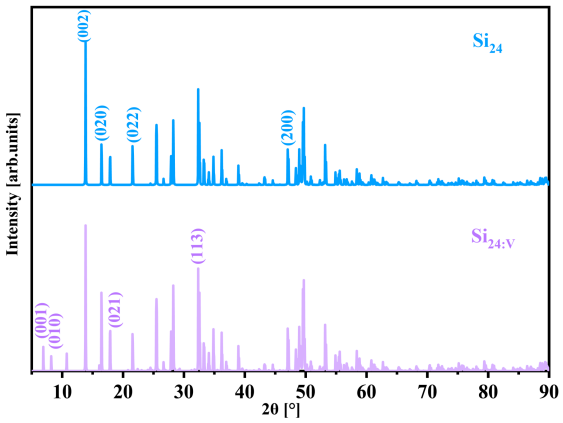

Fig. 6. Simulated XRD patterns for *Cmcm* Si_{24} and *Cmcm* Si_{24}:V; X-ray wavelength of 1.5406 Å and a copper source were used for simulation in this work.

namely (001), (010), (011), and (01-1), which appear at the diffraction angles of 6.91°, 8.21°, and 10.73°, respectively. It also has the major diffraction peaks of (002), (020), (021), (022), and (113) at the diffraction angles of 13.84°, 16.46°, 17.87°, and 21.57°. The difference is that when the diffraction angle is 32.35°, four diffraction peaks simultaneously appear in the XRD patterns of *Cmcm* Si_{24}:V. They are (1-1-3), (1-13), (113), and (11-3) peaks, respectively. These X-ray diffraction characteristics are of great significance and provide guidance for analyzing the structure of *Cmcm* Si_{24} and *Cmcm* Si_{24}:V in subsequent experiments.

4. Conclusions

In general, this work utilized the first principle calculation based on density functional theory to investigate the effect of the presence of *Cmcm* Si_{24}:V on physical properties. The results show that the presence of vacancy does not affect the crystal lattice parameters, but the density of *Cmcm* Si_{24}:V is larger than *Cmcm* Si_{24}. The elastic constants satisfied the orthorhombic symmetry generalized Born's mechanical stability criteria and demonstrated the mechanical stability for *Cmcm* Si_{24} and *Cmcm* Si_{24}:V. The lower formation energy of *Cmcm* Si_{24}:V illustrated the synthesized possibility. Moreover, 3D surface constructions of Young's modulus of *Cmcm* Si_{24} and *Cmcm* Si_{24}:V show that they have varying degrees of mechanical anisotropy. According to the electronic band structures, *Cmcm* Si_{24} has indirect band gaps of 1.08 eV. Furthermore, the *Cmcm* Si_{24}:V exhibits metallic characteristics in electronic band structures. These results indicated that the presence of vacancy of *Cmcm* Si_{24} has a great effect on electronic band structure. In addition, the high ELF values with symmetric shapes at the bond centers indicated strong covalent silicon–silicon bonds of the vacancy structure of *Cmcm* Si_{24}. The effective mass of electrons and holes of *Cmcm* Si_{24} is smaller than that of diamond-Si along the *a* direction and larger than that along the *b* and *c* directions. Finally, this work studied the X-ray diffraction characteristics for *Cmcm* Si_{24} and *Cmcm* Si_{24}:V, which has important guiding significance for the analysis in subsequent experiments. The XRD patterns for *Cmcm* Si_{24} and *Cmcm* Si_{24}:V are very close after 13.84°.

The data that support the findings of this study are available from the corresponding author upon reasonable request.

Acknowledgments

This work was supported by the National Natural Science Foundation of China (No. 61804120), China Postdoctoral Science Foundation (No. 2019TQ0243, No. 2019M663646), Key Science and Technology Innovation Team of Shaanxi Province (2022TD-34), Natural Science Basic Research Program of Shaanxi (Program No.2021JQ-515), Key scientific research plan of Education Department of Shaanxi Provincial Government (Key Laboratory Project) (No. 20JS066), Young Talent fund of University Association for Science and Technology in Shaanxi, China (No. 20190110), National Key R&D Program of China (No. 2018YFB1502902), and Key Program for International S&T Cooperation Projects of Shaanxi Province (No. 2019KWZ-03).

References

[1] C. Bai, C. Chai, Q. Fan, Y. Liu, Y. Yang, *Materials* **10**, 441 (2017).

[2] H. Liu, M. Xing, Q. Fan, *Diamond Relat. Mater.* **135**, 109854 (2023).

[3] Q. Fan, Y. Sun, Y. Zhao, Y. Song, S.Yun, *Phys. Scr.* **98**, 015701 (2022).

[4] R. Zhao, Q. Fan, R. Yang, Y. Song, X. Yu, S. Yun, *J. Mater. Res. Technol.* **23**, 4244 (2023).

[5] M. Xing, X. Li, *Diamond Relat. Mater.* **131**, 109592 (2023).

[6] M. Xing, X. Li, *J. Electron. Mater.* **52, 2071 (2023)**.

[7] Q. Fan, H. Wang, Y. Song, W. Zhang, S.Yun, *Comput. Mater. Sci.* **178**, 109634 (2020).

[8] M. Amsler, S. Botti, M. Marques, T. Lenosky, S. Goedecker, *Phys. Rev. B* **92**, 014101 (2015).

[9] S. Botti, J. Flores-Livas, M. Amsler, S. Goedecker, M. Marques, *Phys. Rev. B* **86**, 121204 (2012).

[10] Q. Fan, C. Li, R. Yang, X. Yu, W. Zhang, S. Yun, *J. Solid State Chem.* **294**, 121894 (2021).

[11] Q. Fan, H. Liu, L. Jiang, X. Yu, W. Zhang, S. Yun, *Diamond Relat. Mater.* **116**, 108426 (2021).

[12] Y. Luo, C. Ren, Y. Xu, J. Yu, S. Wang, M. Sun, *Sci. Rep.* **11** , 19008 (2021).

[13] Q. Fan, H. Liu, R. Yang, X. Yu, W. Zhang, S. Yun, *J. Solid State Chem.* **300**, 122260 (2021).

[14] Y. Zhao, W. Zhang, Q. Fan, *Commun. Theor. Phys.* **71**, 1036 (2019).

[15] Q. Fan, H. Liu, L. Jiang, W. Zhang, Y. Song, Q. Wei, X. Yu, S. Yun, *Nanotechnol. Rev.* **10**, 1266 (2021).

[16] Q. Fan, N. Wu, R. Yang, W. Zhang, X. Yu, S. Yun, *J. Appl. Phys.* **131**, 055703 (2022).

[17] Q. Fan, B. Hao, Y. Zhao, Y. Song, W. Zhang, S. Yun, *Vacuum* **199**, 110952 (2022).

[18] Y. Oh, I. Lee, S. Kim, J. Lee, K. Chang, *Sci. Rep.* **5**, 18086 (2015).

[19] C. He, C. Zhang, J. Li, X. Peng, L. Meng, C. Tang, J. Zhong, *Phys. Chem. Chem. Phys.* **18**, 9682 (2016).

[20] M. Amsler, S. Botti, M. Marques, T. Lenosky, S. Goedecker, *Phys. Rev. B* **92**, 014101 (2015).

[21] Q. Fan, C. Chai, Q. Wei, H. Yan, Y. Zhao, Y. Yang, X. Yu, Y. Liu, M. Xing, J. Zhang, R. Yao, *J. Appl. Phys.* **118**, 185704 (2015).

[22] I. Lee, Y. Oh, S. Kim, J. Lee, K. Chang, *Comput. Phys. Commun.* **203**, 110 (2016).

[23] Q. Fan, C. Chai, Q. Wei, P. Zhou, J. Zhang, Y. Yang, *Materials* **9**, 284 (2016).

[24] A. Mujica, C. Pickard, R. Needs, *Phys. Rev. B* **91**, 214104 (2015).

[25] Q. Fan, C. Chai, Q. Wei, Y. Yang, *Phys. Chem. Chem. Phys.* **18**, 12905 (2016).

[26] Y. Guo, Q. Wang, Y. Kawazoe, P. Jena, *Sci. Rep.* **5**, 14342 (2015).

[27] D. Kim, S. Stefanoski, O. Kurakevych, T. Strobel, *Nat. Mater.* **14**, 169 (2015).

[28] Q. Fan, R. Niu, W. Zhang, W. Zhang, Y. Ding, S. Yun, *ChemPhysChem* **20**, 128 (2019).

[29] A. Oreshonkov, E. Roginskii, V. Atuchin, *J. Phys. Chem. Solid.* **137**, 109219 (2020).

[30] Q. Fan, H. Peng, W. Zhang, X. Yu, S. Yun, *J. Solid State Chem.* **305**, 122641 (2022).

[31] W. Zhang, C. Chai, Q. Fan, Y. Song, Y. Yang, *J. Phys. Condens. Matter* **32**, 355701 (2020).

[32] Q. Fan, W. Zhang, Y. Song, W. Zhang, S. Yun, *Semicond. Sci. Technol.* **35**, 055012 (2020).

[33] X. Cai, Q. Yang, Y. Pang, M. Wang, *Comput. Mater. Sci.* **173**, 109441 (2020).

[34] Q. Fan, C. Chai, Q. Wei, Y. Yang, *Phys. Chem. Chem. Phys.* **18**, 12905 (2016).

[35] D. Kim, S. Stefanoski, O. Kurakevych, T. Strobel, *Nat. Mater.* **14**, 169 (2015).

[36] S.J. Clark, M. Segall, C. Pickard, P. Hasnip, *Z. Kristallogr.* **220**, 567 (2005).

[37] P. Hohenberg, W. Kohn, *Phys. Rev.* **136**, B864 (1964).

[38] W. Kohn, L. Sham, *Phys. Rev.* **140**, A1133 (1965).

[39] J.P. Perdew, K. Burke, M. Ernzerhof, *Phys. Rev. Lett.* **77**, 3865 (1996).

[40] B. Pfrommer, M. C^ot´e, S. Louie, M. Cohen, *J. Comput. Phys.* **131**, 233 (1997).

[41] D. Vanderbilt, *Phys. Rev. B* **41**, 7892 (1990).

[42] H. Monkhorst, J. Pack, *Phys. Rev. B* **13**, 5188 (1976).

[43] R. Hill, *Proc. Phys. Soc. A* **65**, 349 (1952).

[44] A. Krukau, O. Vydrov, A. Izmaylov, G. Scuseria, *J. Chem. Phys.* **125**, 224106 (2006).

[45] Jia W, Fu J, Cao Z, et al. *J. Comput. Physics* **251**, 102 (2013).

[46] W. Jia, Z. Cao, L. Wang et al. *J. Comput. Phys. Commun.* **184**, 9 (2013).

[47] B. Silvi, A. Savin, *Nature* **371**, 683 (1994).

[48] A. Becke, K. Edgecombe, *J. Chem. Phys.* **92**, 5397 (1990).

[49] J. Linghu, L. Shen, M. Yang, S Xu, Y. Feng, *J. Phys. Chem. C* **121**, 15574 (2017).

[50] F. Mouhat, F X. Coudert, *Phys. Rev.* **90**, 224104 (2014).

[51] J. Dabrowski, G. Kissinger, *Phys. Rev. B* **92**, 144104 (2015).